



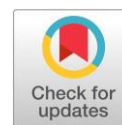
The impact of dimethylformamide on the synthesis of graphene quantum dots derived from graphene oxide

Khuong T. Truong^{ab} , Thach H. Pham^{ab}, Khai V. Tran^{ab*} 

a: Faculty of Materials Technology, Ho Chi Minh City University of Technology (HCMUT), Ho Chi Minh 700000, Vietnam

b: Vietnam National University Ho Chi Minh City (VNU-HCM), Ho Chi Minh 700000, Vietnam

* Corresponding author: tvkhai1509@hcmut.edu.vn



This paper belongs to a Regular Issue.

Abstract

Graphene quantum dots (GQDs) have garnered immense interest in recent years due to their unique optical, electrical, and chemical properties, making them promising candidates for various applications in optoelectronics, bioimaging, and sensing. However, enhancing the control over the size, surface chemistry, and optical properties of GQDs remains a significant challenge. In this study, a novel recipe was proposed to successfully synthesize various GQDs via a typical solvothermal process, which has proven to be a versatile and scalable approach. In addition to the main ingredient – graphene oxide suspension, dimethylformamide (DMF) and hydrogen peroxide serving as a cutting agent were added to the reaction mixture. This synthesis method was found to be more promising than the reference one in which DMF was replaced by double distilled water. Through systematic experimentation, we demonstrated that the addition of DMF enables the successful GQD production over a wider range of reaction times; hence, the UV absorption band and photoluminescence properties of GQDs can be better adjusted. The dependence of photoluminescence on the excitation wavelength was observed in the as-prepared materials as they were excited with a range of wavelengths from 360 to 480 nm. The obtained insights not only advance our understanding of GQD synthesis but also open up avenues for tailoring their properties for specific applications.

Keywords

graphene quantum dots
graphene oxide
solvothermal
photoluminescence
dimethylformamide

Key findings

- A solvothermal process to obtain GQDs was applied successfully.
- For samples prepared without DMF, the viable range of reaction time is remarkably narrow.
- For GQDs synthesized with DMF, there are many remarkable effects of solvothermal time on their optical behaviours.

© 2023, the Authors. This article is published in open access under the terms and conditions of the Creative Commons Attribution (CC BY) license (<http://creativecommons.org/licenses/by/4.0/>).

Received: 01.09.23
Revised: 04.10.23
Accepted: 05.10.23
Available online: 10.10.23

1. Introduction

The extraordinary structural, optical, and electronic characteristics of graphene have garnered significant interest from the scientific and technological community [1, 2]. Nevertheless, the absence of an optical bandgap in graphene hinders the luminescence ability, consequently impeding the advancement of new technologies that rely on this property [3]. This promoted many works aiming to adjust the band gap of graphene-based structures through many approaches including the formation of edge defects or modifications of the shape and size of the material.

In such a context, graphene-based quantum dots or graphene quantum dots (GQDs), which are nanoscale fragments of graphene, have attracted much attention since their exclusive fluorescent properties were reported [4]. When material size reaches 10 nm, quantum confinement and edge effects become dominant, and, consequently, GQDs not only exhibit excitation wavelength-dependent fluorescence [5] but also display the chemical and physical properties distinct from the other carbon-based materials like carbon dots, carbon nanotubes, fullerene, and graphene [6, 7]. Besides, this new type of fluorophores also

possesses advantageous features, such as good water solubility, low toxicity, and biocompatibility [8–10]. Some exceptional characteristics of GQDs, which surpass traditional semiconductor quantum dots, have sparked interest in numerous potential applications. These applications include but are not limited to energy conversion and storage [11–13], photodetectors [14, 15], sensors [16, 17], bioimaging [18, 19], drug carriers [20, 21], and catalytic processes [22–24].

However, despite the significant advantages and potential applications of GQDs, further research is needed to improve their properties to meet specific application demands. In fact, there are still many obstacles that have yet to be adequately addressed. The first one is the low product yield of many prevalent methods (mostly less than 10%) [25], which urges the exploration of new methods. Besides, intrinsic properties of GQDs, such as band gap, closely correlate with their size, shape, surface modifications and related parameters [26, 27]. Therefore, another major challenge is to accurately control such factors to better manipulate GQDs for specific purposes. In order to meet this demand, the details of the fabrication methods are supposed to play a critical role.

Herein, we present a solvothermal method to produce GQDs from graphene oxide (GO), hydrogen peroxide and dimethylformamide (DMF). The reaction conditions were fixed except for the reaction time. The volume ratio between GO suspension and DMF was kept at 2:1. To make comparisons, the same procedures were replicated, but DMF was replaced by double distilled water (DDW). The purifying process is straightforward, involving centrifugation, evaporation and redissolution, and no tedious dialysis process was carried out.

2. Materials and Methods

2.1. Materials

Graphite (Gi, with particle size <20 μm) and methylene blue trihydrate (MB, $\text{C}_{16}\text{H}_{18}\text{ClN}_3\text{S}\cdot 3\text{H}_2\text{O}$) were ordered from Sigma Aldrich Co. Ltd., USA. Potassium permanganate (KMnO_4) and hydrogen peroxide (H_2O_2) were purchased from Duc Giang Chemicals Group JSC, Vietnam. Sulfuric acid (H_2SO_4), phosphoric acid (H_3PO_4), hydrochloric acid (HCl), and dimethylformamide (DMF, $(\text{CH}_3)_2\text{NCH}$) were obtained from Xilong Scientific Co. Ltd., China. All chemicals were used without further purification.

2.2. Synthesis of GO

The modified Hummers' method was employed to synthesize graphene oxide (GO) from Gi [28, 29]. In short, a solution comprising 120 mL of H_2SO_4 and 13.3 mL of H_3PO_4 was added with 1.0 g of pure graphite powder and vigorously stirred at low temperatures. Following this, 6.0 g of KMnO_4 was added to the mixture that was later stirred for 12 h at 50 $^\circ\text{C}$. Subsequently, the mixture was cooled naturally to room temperature before being slowly treated with 5 mL of

30% H_2O_2 and 166 mL DDW, leading to the color alteration from brown to yellow. The resulting mixture was initially centrifuged at 5000 rpm for 10 min. While the supernatant was removed, the residuals were further washed with 1 M HCl and DDW several times. Finally, the GO suspension was obtained after ultrasonication conditions (35 kHz, 180 W) in an ice bath for 5 h.

2.3. Synthesis of GQDs

Solvothermal treatment was utilized in the synthesis of GQDs from GO. In a typical procedure, a mixture of 4 mL of 30% hydrogen peroxide and 40 mL of a 0.4 mg/mL aqueous suspension of GO was prepared, followed by the addition of 20 mL of DMF (for Q1a, Q2a, Q3a, or DDW for Qo). After stirring for 15 min, the resulting brownish mixture was transferred to a Teflon-lined stainless-steel autoclave. Subsequently, the autoclave was placed in an oven at 170 $^\circ\text{C}$ and heated for A min (A = 90 for Q1a; A = 110 for Q2a; A = 130 for Q3a). Afterwards, the autoclave was naturally cooled to room temperature. The mixture was then centrifuged at 12000 rpm for 10 min to get rid of the black sediment before the pale yellow supernatant underwent vacuum evaporation before the residue was re-dissolved in DDW to gain GQD dispersion.

In order to make systematic comparisons, different GQDs were prepared via an identical procedure, but 20 mL of DMF was replaced by 20 mL of double distilled water. As a result, GQDs Q1b, Q2b and Q3b were obtained after the heating stage of 90, 110, and 130 min, respectively.

2.4. Characterization

X-ray diffraction (XRD) patterns were acquired by using a D2 Phaser (Bruker) with Cu $\text{K}\alpha$ radiation ($\lambda = 1.5406 \text{ \AA}$). Raman measurements were performed using a Horiba XploRA ONE spectrometer in which a laser source with $\lambda = 632.8 \text{ nm}$ was employed as the excitation source. Fourier transform infrared spectroscopy (FTIR) spectra ranging from 500 to 4000 cm^{-1} were obtained by using a Platinum ATR Alpha II spectrometer (Bruker, Germany). Ultraviolet-visible (UV-Vis) spectra were obtained using a STECH 754N UV-Vis spectrophotometer, while photoluminescence (PL) spectra were recorded at room temperature in aqueous solutions using a Cary Eclipse Fluorescence Spectrometer (Agilent Technologies, Inc., USA).

3. Results and Discussion

3.1. Visible results of samples

Many differences between the two GQD series of GQDs can be observed easily with the naked eye. Regarding Q1b, the solution became transparent right after the centrifuge step. Then, a 365 nm UV lamp was used to illuminate the concentrated solution of Q1b in a quartz cuvette, and nearly no luminescence signal was witnessed. This means that such an experiment was unsuccessful, and almost no GQD was created.

According to a previous report [30], such a result can be attributed to insufficient reaction time. In such a case, the cutting process might not reach the threshold where a considerable proportion of GO sheets could turn into GQDs, which explains the facts that the supernatant of Q1b in centrifuge tubes was transparent and the PL phenomenon did not take place under a 365 nm UV source. By contrast, a colourless solution of Q3b was revealed right after the heating stage. It was highly possible that most GQDs in this sample were destroyed as the solvothermal reaction was ceased too late, which was confirmed by the fact that such a colourless solution showed no PL under a 365 nm UV light.

Among the 3 configurations, only Q2b was found promising, since this solution emitted green light under the excitation of a 365 nm light. After the cooling step, the Teflon liner of Q2b was opened, and the mixture inside was brownish yellow. Although a small amount of sediment was removed by centrifugation, the final product of Q2b retained this colour (Figure 1), and it was less transparent than Q1a, Q2a or Q3a. These visual effects closely correlate with analysis results shown in the following sections. Although the detailed synthesis conditions in this work are relatively different from reported works utilizing the same chemicals, the observations show many similarities [30, 31], confirming the viability of the proposed method.

In terms of experiments involving the usage of DMF, the outcomes were obviously different. Q1a, Q2a, and Q3a solutions possessed a pale yellow colour (Figure 1) after the purifying process and exhibited varying colours when they were exposed under a UV lamp with a wavelength of 365 nm. Such optical properties will be discussed thoroughly below.

3.2. Structural analysis

XRD is a standard method used to confirm the formation of GQDs derived from GO. As can be seen in Figure 2, there are apparent differences between the XRD patterns of GQD samples, GO and initial graphite powder. The XRD pattern for graphite powder exhibited two characteristic peaks centered at $\sim 26.7^\circ$ and $\sim 54.8^\circ$ corresponding to the (002) and (004) planes, respectively. Based on the classic Bragg's equation, d_{002} of 0.33 nm could be calculated. At the same time, the XRD pattern of GO presented the characteristic (001) peak at $\sim 10.95^\circ$, meaning that the average space between the planes was expanded to about 0.81 nm due to the oxidation process. These characteristics agree with the previous reports [32, 33]. By contrast, there was a prominent peak with 2θ of approximately 24.1° in the XRD pattern of Q2b, corresponding to the (002) plane with a d -spacing of 0.37 nm. Besides, there was a small peak at around 14.2° in this XRD pattern representing residual GO and explaining the brownish yellow color of the suspension. The XRD patterns of Q1a, Q2a and Q3a also depicted a similar peak with a minor shift to about 23.9° . Such alterations of diffraction peaks between GO and GQDs helped confirm the formation of targeted materials. Additionally, the restoration of the

hexagonal honeycomb lattice after reduction was clearly evident in the proximity of (002) peaks in GQDs to that of raw graphite powder ($2\theta = 26.6^\circ$) [34]. However, the d -spacing values of GQDs are still larger than that of graphite indicating the presence of oxygen-containing functional groups. In addition, the average sp^2 domain size of such GQDs can be estimated via the Debye-Scherrer formula:

$$D = \frac{0.9\lambda}{\beta \cos\theta} \quad (1)$$

where D (nm) is the average sp^2 domain size of the synthesized GQDs, λ (nm) is the wavelength of X-ray, θ (rad or degree) is the diffraction angle, and β (rad) is the full width at half maximum (FWHM). According to this equation, the average sp^2 domain size of GO is around 5 nm, whereas that of GQDs is about 1 nm, which implies that graphene sheets in GQDs were cut into the nanoscale GQDs.



Figure 1 Digital pictures of GQD samples.

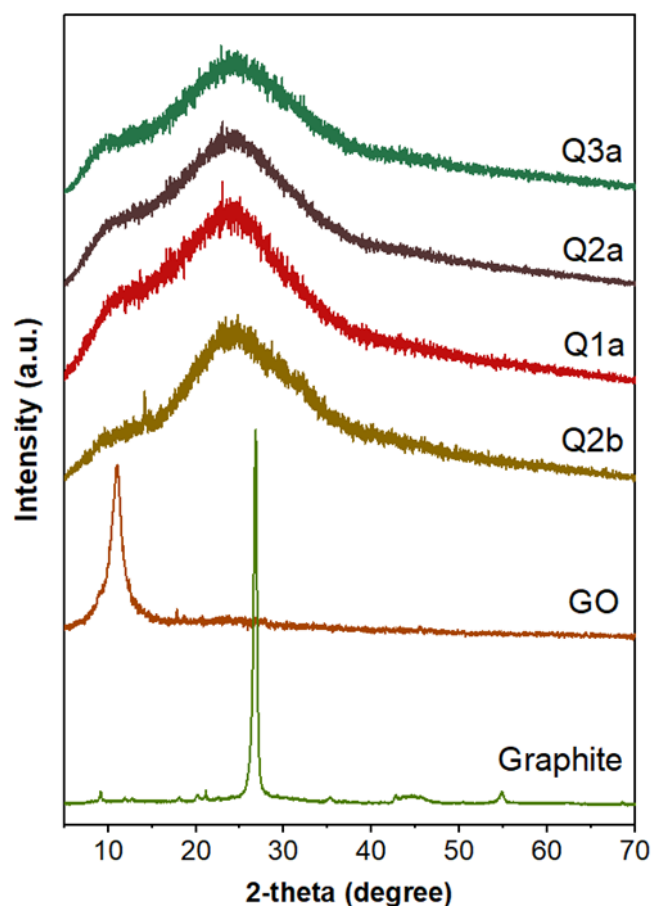


Figure 2 XRD patterns of graphite, prepared GO and GQDs.

Figure 3 depicts the FTIR spectra of GQD samples proving the presence of many similar functional groups. The strong band associated with the stretching vibration of the -OH group emerged at $\sim 3430\text{ cm}^{-1}$ for Q2b, while less intensive bands at 3380 cm^{-1} related to O-H bonds were observed in the other FTIR spectra. The signals for the absorption of C-H stretching vibrations were located at 3174 and 3293 cm^{-1} for Q2b and the other samples, respectively. The presence of -C=O groups was confirmed by the absorption peaks at 1758 cm^{-1} (for Q2b) and 1718 cm^{-1} (for the other ones) [35]. The C=C bonds of the aromatic rings could be assigned to the bands at $1625\text{--}1655\text{ cm}^{-1}$, whereas the bands centered at 1315 and 1385 cm^{-1} were attributed to the vibration of C-O bonds [36]. It was reasonable to expect the appearance of -COOH and -OH groups, as quantum dots were obtained by separating sp^2 domains of GO into nanoscale structures. Besides, the peak centered at 827 cm^{-1} only appeared in FTIR spectra of Q2b and could be ascribed to bond deformation in epoxy groups (C-O-C) [37, 38]. In addition, a weak band whose position varied between $1247\text{--}1253\text{ cm}^{-1}$ for Q1a, Q2a and Q3a might arise due to the absorption of C-N bonds. As temperature rises higher than boiling point ($153\text{ }^\circ\text{C}$), DMF can partially decay to form carbon monoxide and dimethylamine ($\text{NH}(\text{CH}_3)_2$) [39], and such a nitrogen-containing substance might interact with graphene lattice to produce C-N bonds [40].

Raman spectroscopy was applied as it plays a crucial role in evaluating the structural features of graphene-based materials. The distinctive information about D and G bands is mainly used for analytical purposes. D band is linked to disorder and defects in the hexagonal lattice, while G band originates from the vibrations of sp^2 carbon atoms [41]. The intensity ratio between D and G bands (I_D/I_G ratio) can be calculated to estimate the degree of disorder [42]. In Figure 4, Raman spectra of GQDs are presented with two prominent peaks observed in all samples. Table 1 summarizes the positions of peaks corresponding to D band and G band as well as the ratio of I_D/I_G for each Raman spectrum.

In general, D band was found between 1344 and 1362 cm^{-1} , while G band appeared at about $1585\text{--}1602\text{ cm}^{-1}$. Interestingly, Q2b showed the highest value of I_D/I_G (1.11). At the same time, the remaining samples involving DMF in the synthesis process resulted in smaller I_D/I_G figures which slightly reduced (from 1.07 to 0.97) as the reaction time rose from 90 to 130 min. This result suggests that the increasing solvothermal period facilitated the reduction process leading to a decline in the sp^3 hybridized proportion of carbon-to-carbon bonds and carbon-to-oxygen bonds related to epoxy and hydroxyl groups [43]. It can be explained by the fact that the longer the solvothermal period, the more carbon monoxide, a reducing agent, is generated by the decomposition of DMF.

3.3. Optical behaviours of GQDs

In order to acquire initial information about the fluorescence properties of GQDs, their suspensions were diluted

with DDW in a quartz cuvette, which was later used for UV-Vis absorption analysis and exposed to 365 nm UV irradiation to take photographs (Figure 5).

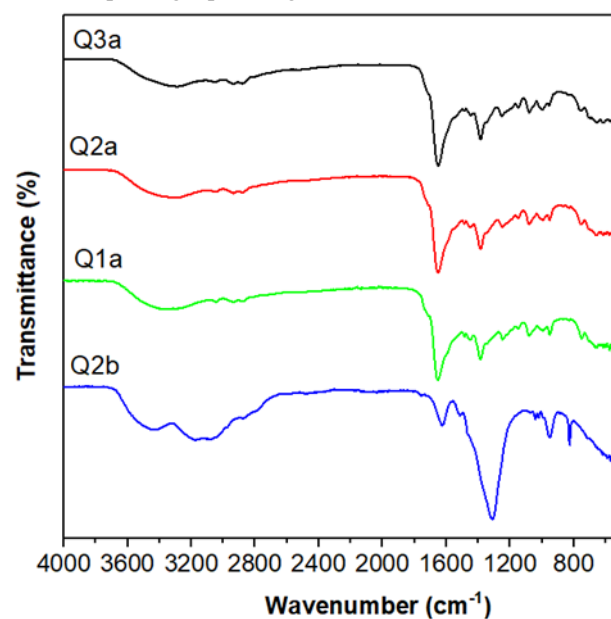


Figure 3 FTIR spectra of GQDs.

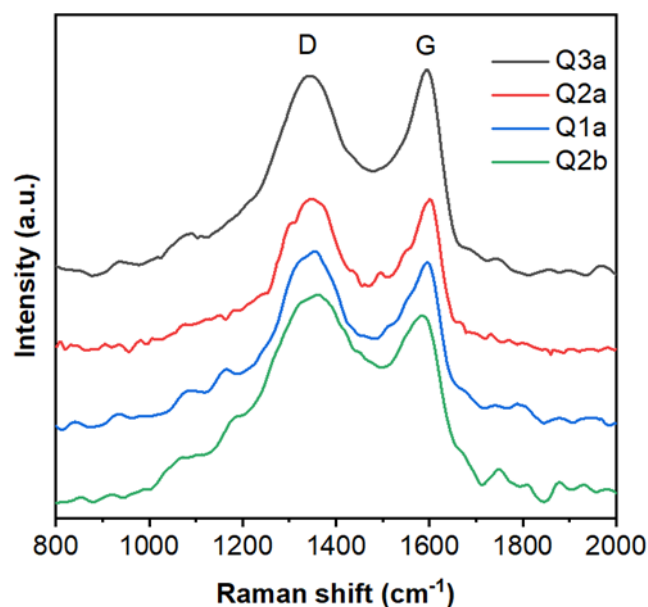
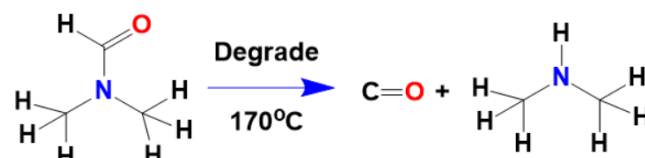


Figure 4 Raman spectra of GQDs.



Scheme 1 Illustration of DMF decomposition reaction.

Table 1 Positions of D and G bands in Raman spectra of the synthesized GQDs and the ratio between I_D and I_G .

Sample	D band (cm^{-1})	G band (cm^{-1})	I_D/I_G
Q1a	1355	1595	1.07
Q2a	1348	1602	1.00
Q3a	1344	1594	0.97
Q2b	1362	1585	1.11

Suspensions of Q2b and Q1a exhibited green colors, while those of Q2a and Q3a emitted bright blue light.

Light absorption properties of GQD samples are shown in Figure 6. Q1a exhibited a broad absorption band in the ultraviolet region, with the center at around 239 nm. The absorption peaks of Q2a and Q3a were narrower and centered at nearly the same position, approximately 237 nm, and that of Q2b was situated at 233 nm. These peaks correlate with the $\pi \rightarrow \pi^*$ transition caused by the presence of sp^2 hybridized carbons [44]. Besides, a small shoulder peak was observed at around 326 nm in the UV-Vis spectrum of Q1a, whereas such a feature appeared at about 317 nm in the spectra of Q2a and Q3a and was less obvious in that of Q2b. The absorption tail at 300–800 nm refers to the $n \rightarrow \pi^*$ transition associated with the existence of oxygen functional groups in GQDs [44].

PL characteristics of GQDs, the primary concern of most related optoelectronic applications, were measured by utilizing numerous excitation wavelengths from 360 to 480 nm (Figure 7). Table 2 demonstrates the PL band and emission energy of prepared GQDs for each excitation wavelength. For Q1a, Q2a and Q3a, their suspensions showed excitation-dependent PL emission in aqueous solution. There were shifts of the PL peaks to longer wavelengths as the excitation increased, and their intensities started dropping significantly when the excitation wavelength exceeded 400 nm.

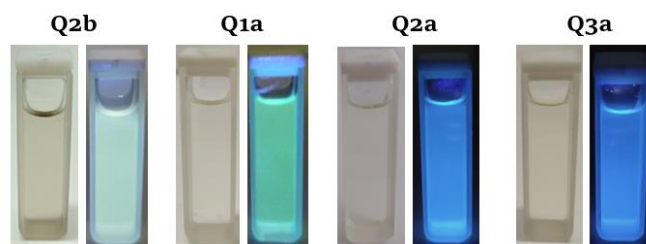


Figure 5 Digital pictures of GQD samples dispersed in a quartz cuvette used to measure UV-Vis spectra: under white neon light (left) and 365 nm UV light (right).

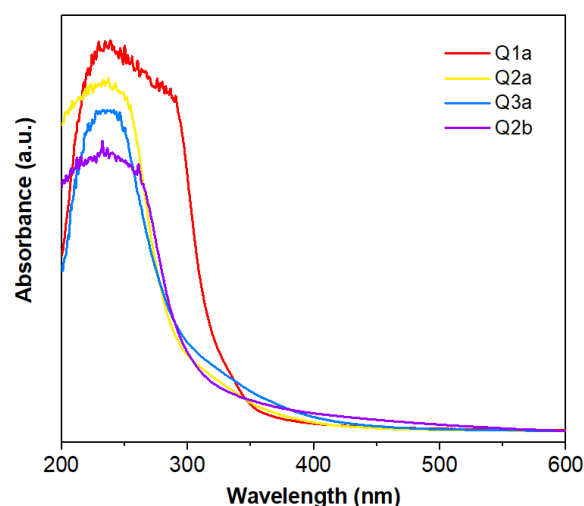


Figure 6 UV-Vis absorption spectra of GQD samples.

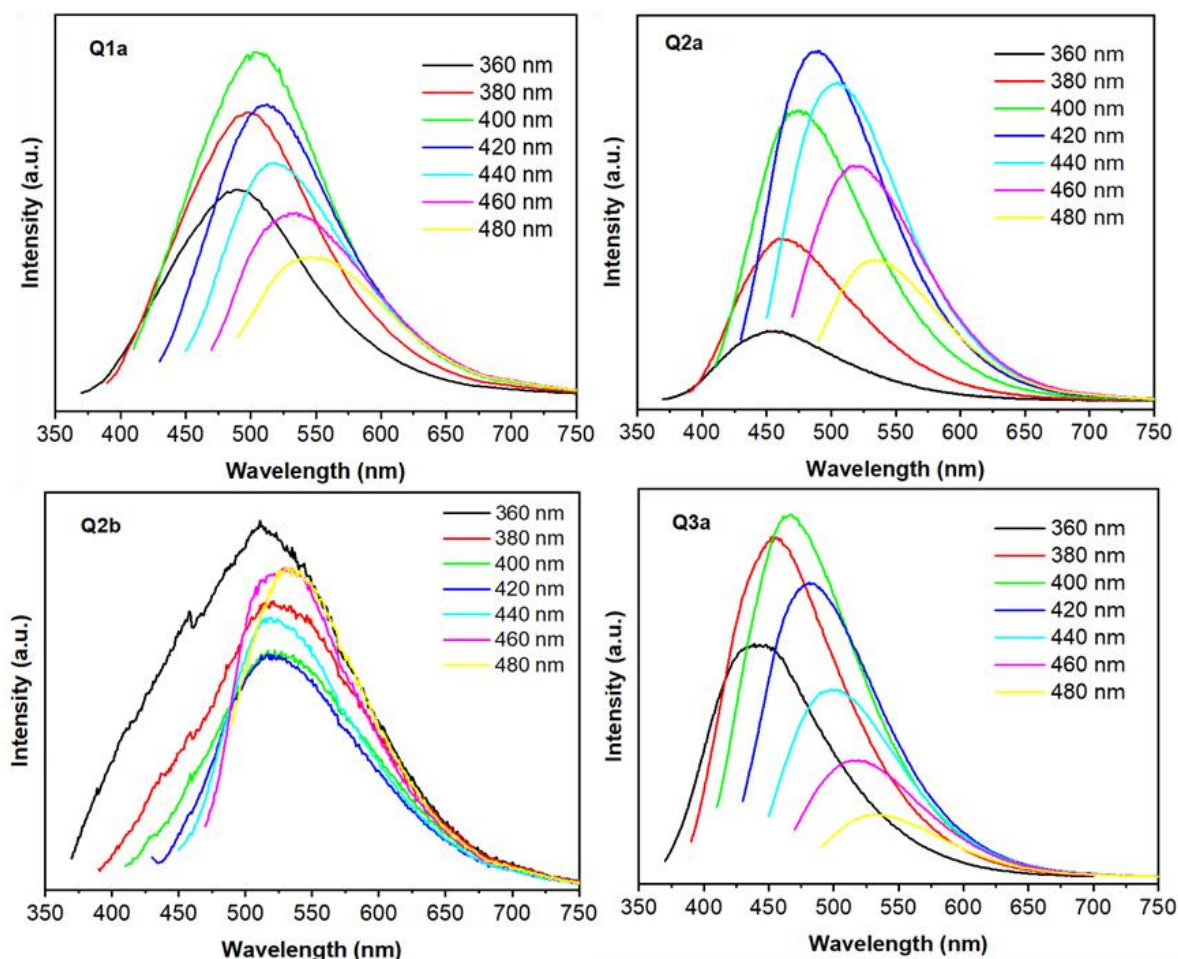


Figure 7 PL spectra of GQDs excited by different wavelengths ranging from 360 to 480 nm.

Table 2 Emission peaks of PL spectra and respective emission energy.

Excitation wavelength (nm)	Excitation energy (eV)	Emission peak (nm)				Emission energy (eV)			
		Q1a	Q2a	Q3a	Q2b	Q1a	Q2a	Q3a	Q2b
360	3.44	490	453	442	511	2.53	2.74	2.81	2.43
380	3.26	498	462	455	521	2.49	2.68	2.72	2.38
400	3.10	505	474	467	521	2.46	2.62	2.65	2.38
420	2.95	512	488	482	521	2.42	2.54	2.57	2.38
440	2.82	518	503	501	519	2.39	2.46	2.47	2.39
460	2.70	532	518	517	532	2.33	2.39	2.40	2.33
480	2.58	546	532	532	532	2.27	2.33	2.33	2.33

The PL spectra of QD1a and Q3a exhibited the strongest peak at 505 and 467 nm, respectively, whereas the most intensive peak in the PL spectra for Q2a was centered at 488 nm, corresponding to the 400 nm excitation wavelength. The PL spectra of Q2b, which were recorded in similar conditions, displayed the highest intensity with an excitation wavelength of 360 nm. As for the excitation wavelength of 360 nm, the PL spectrum of Q2b showed a shoulder peak at 458 nm. Even though such a peak was less noticeable in the other spectra, its presence implies that Q2b suspension may contain a higher amount of impurities compared to the other samples. Although such emission peaks tended to move from ~511 to ~532 nm as excitation energy reduced, the regularity of peak shift and emission seems inconsistent. According to previous studies, the blue and green emissions that GQDs behave originate from size confinement, edge defects and functional groups of GQDs [8, 45, 46]. Therefore, the asymmetry of the PL spectrum for the synthesized GQDs could be explained as the overall consequence of the factors mentioned above. In terms of Q1a and Q2b, the presence of oxygen functional groups (C–O, C=O, and O–C=O) on their surfaces could be assigned to green luminescence [47], whereas armchair edges seemed to be the cause of blue luminescence in Q2a and Q3a samples having the lower amount of oxidation [44]. The above results once again confirmed the vital role of synthesis parameters in the optical behaviors of produced materials.

4. Limitations

In this study, a hydrogen peroxide solution was added to dramatically reduce the reaction time compared with procedures not using cutting agents [34, 48], while the appearance of DMF brings about undeniable benefits. However, this also raises an issue as such solvents have high boiling points (above 150 °C), making removing their residues more time- and energy-consuming. Besides, the purity can be further improved by centrifuging GQD suspensions with higher angular velocity to remove the remaining GO completely. It would be more efficient to apply an advanced centrifuge where the rotating speed can reach 15000 rpm or more in a cooled atmosphere. This can not only allow the separation of smaller and lighter GO pieces but also prevent the plastic containers from melting or distorting. Moreover, further effort should be made to precisely calculate the

quantum yields of the synthesized GQDs, which allows a deeper comprehension of their behavior as well as more reasonable comparisons with the previous studies.

5. Conclusions

We suggested a solvothermal procedure involving DMF and hydrogen peroxide to produce GQDs from GO and successfully confirmed its viability. Such nanoparticles exhibited blue to green fluorescence under irradiation with a 365 nm UV light. The FTIR spectra of synthesized GQDs indicated the presence of many functional groups, including hydroxyl, carbonyl, epoxy, and carboxyl. The addition of DMF resulted in obvious differences in the synthesis parameters and properties of GQDs, as compared to the reference samples. The enlargement of viable heating time is especially important. As for Q1a, Q2a and Q3a, nitrogen atoms might chemically link to the graphene lattice, which was confirmed by the appearance of the C–N band at around 1247–1253 cm^{-1} . When the reaction time rose, the UV absorption band of such GQDs tended to shrink, and their PL emission bands shifted from green to blue region of light (from around 505 to 467 nm for 400 nm excitation wavelength). When each GQD suspension was excited by different wavelengths from 360 to 480 nm, it revealed the most substantial PL emission peak with an excitation wavelength of 380 or 400 nm, and the intensities of emission peaks with larger excitation wavelengths fell noticeably. Owing to the DMF addition, these alterations of material properties were obtained simply by extending the heating period by 20 or 40 min, which implies the possibility of more precise tailoring of the GQD characteristics for specific applications, especially ones in optoelectronics.

• Supplementary materials

No supplementary materials are available.

• Funding

This research had no external funding.

• Acknowledgments

We acknowledge Ho Chi Minh City University of Technology (HCMUT), VNU-HCM, for supporting this study.

● Author contributions

Conceptualization: K.V.T., K.T.T.

Data curation: K.T.T., T.H.P.

Formal Analysis: K.T.T., K.V.T.

Investigation: K.T.T., T.H.P.

Methodology: K.T.T., K.V.T.

Project administration: K.V.T.

Resources: K.T.T., K.V.T.

Software: K.T.T., T.H.P.

Supervision: K.V.T.

Validation: K.T.T.

Visualization: K.T.T., T.H.P.

Writing – original draft: K.T.T.

Writing – review & editing: K.T.T., K.V.T.

● Conflict of interest

The authors declare no conflict of interest.

● Additional information

Author ID:

Khai V. Tran, Scopus ID [36816618000](https://orcid.org/0009-0001-3681-6661).

Websites:

Ho Chi Minh City University of Technology (HCMUT), <https://hcmut.edu.vn/en>;

Vietnam National University Ho Chi Minh City (VNU-HCM), <https://vnuhcm.edu.vn>.

References

- Allen M J, Tung V C, Kaner R B. Honeycomb Carbon: A Review of Graphene. *Chem Rev.* 2010;110(1):132–145. doi:[10.1021/cr900070d](https://doi.org/10.1021/cr900070d)
- Balandin A A, Ghosh S, Bao W, Calizo I, Teweldebrhan D, Miao F, Lau C N. Superior Thermal Conductivity of Single-Layer Graphene. *Nano Lett.* 2008;8(3):902–907. doi:[10.1021/nl0731872](https://doi.org/10.1021/nl0731872)
- Peng J, Gao W, Gupta B K, Liu Z, Romero-Aburto R, Ge L, Song L, Alemany L B, Zhan X, Gao G, Vithayathil S A, Kaiparettu B A, Marti A A, Hayashi T, Zhu J-J, Ajayan P M. Graphene quantum dots derived from carbon fibers. *Nano Lett.* 2012;12(2):844–849. doi:[10.1021/nl2038979](https://doi.org/10.1021/nl2038979)
- Pan D, Zhang J, Li Z, Wu M. Hydrothermal route for cutting graphene sheets into blue-luminescent graphene quantum dots. *Adv Mater.* 2010;22(6):734–738. doi:[10.1002/adma.200902825](https://doi.org/10.1002/adma.200902825)
- Zheng P, Wu N. Fluorescence and Sensing applications of graphene oxide and graphene quantum dots: a review. *Chem Asian J.* 2017;12(18):2343–2353. doi:[10.1002/asia.201700814](https://doi.org/10.1002/asia.201700814)
- Tian P, Tang L, Teng K S, Lau S P. Graphene quantum dots from chemistry to applications. *Mater Today Chem.* 2018;10:221–258. doi:[10.1016/j.mtchem.2018.09.007](https://doi.org/10.1016/j.mtchem.2018.09.007)
- Shen J, Zhu Y, Yang X, Zong J, Zhang J, Li C. One-pot hydrothermal synthesis of graphene quantum dots surface-passivated by polyethylene glycol and their photoelectric conversion under near-infrared light. *New J Chem.* 2012;36(1):97–101. doi:[10.1039/C1NJ20658C](https://doi.org/10.1039/C1NJ20658C)
- Zhu S, Zhang J, Tang S, Qiao C, Wang L, Wang H, Liu X, Li B, Li Y, Yu W, Wang X, Sun H, Yang B. Surface Chemistry routes to modulate the photoluminescence of graphene quantum dots: from fluorescence mechanism to up-conversion bioimaging applications. *Adv Funct Mater.* 2012;22(22):4732–4740. doi:[10.1002/adfm.201201499](https://doi.org/10.1002/adfm.201201499)
- Zhang M, Bai L, Shang W, Xie W, Ma H, Fu Y, Fang D, Sun H, Fan L, Han M, Liu C, Yang S. Facile synthesis of water-soluble, highly fluorescent graphene quantum dots as a robust biological label for stem cells. *J Mater Chem.* 2012;22(15):7461–7467. doi:[10.1039/C2JM16835A](https://doi.org/10.1039/C2JM16835A)
- Wang J, Zhou J, Zhou W, Shi J, Ma L, Chen W, Wang Y, He D, Fu M, Zhang Y. Synthesis, photoluminescence and bio-targeting applications of blue graphene quantum dots. *J Nanosci Nanotechnol.* 2016;16(4):3457–3467. doi:[10.1166/jnn.2016.11817](https://doi.org/10.1166/jnn.2016.11817)
- Ding Z, Hao Z, Meng B, Xie Z, Liu J, Dai L. Few-layered graphene quantum dots as efficient hole-extraction layer for high-performance polymer solar cells. *Nano Energy.* 2015;15:186–192. doi:[10.1016/j.nanoen.2015.04.019](https://doi.org/10.1016/j.nanoen.2015.04.019)
- Liu Q, Sun J, Gao K, Chen N, Sun X, Ti D, Bai C, Cui R, Qu L. Graphene quantum dots for energy storage and conversion: from fabrication to applications. *Mater Chem Front.* 2020;4(2):421–436. doi:[10.1039/C9QM00553F](https://doi.org/10.1039/C9QM00553F)
- Zhang J, Tong T, Zhang L, Li X, Zou H, Yu J. Enhanced performance of planar perovskite solar cell by graphene quantum dot modification. *ACS Sustainable Chem Eng.* 2018;6(7):8631–8640. doi:[10.1021/acssuschemeng.8b00938](https://doi.org/10.1021/acssuschemeng.8b00938)
- Tam TV, Hur SH, Chung JS, Choi WM. Ultraviolet light sensor based on graphene quantum dots/reduced graphene oxide hybrid film. *Sens Actuator A Phys.* 2015;233:368–373. doi:[10.1016/j.sna.2015.07.038](https://doi.org/10.1016/j.sna.2015.07.038)
- Zhuang S, Chen Y, Zhang W, Chen Z, Wang Z. Humidity sensor and ultraviolet photodetector based on carrier trapping effect and negative photoconductivity in graphene quantum dots. *Sci China Phys Mech.* 2017;61(1):014211. doi:[10.1007/s11433-017-9089-6](https://doi.org/10.1007/s11433-017-9089-6)
- Li Y-H, Zhang L, Huang J, Liang R-P, Qiu J-D. Fluorescent graphene quantum dots with a boronic acid appended bipyridinium salt to sense monosaccharides in aqueous solution. *Chem Commun.* 2013;49(45):5180–5182. doi:[10.1039/C3CC40652K](https://doi.org/10.1039/C3CC40652K)
- Kumawat MK, Thakur M, Gurung R B, Srivastava R. Graphene quantum dots from mangifera indica: application in near-infrared bioimaging and intracellular nanothermometry. *ACS Sustainable Chem Eng.* 2017;5(2):1382–1391. doi:[10.1021/acssuschemeng.6b01893](https://doi.org/10.1021/acssuschemeng.6b01893)
- Su Z, Shen H, Wang H, Wang J, Li J, Nienhaus GU, Shang L, Wei G. Motif-designed peptide nanofibers decorated with graphene quantum dots for simultaneous targeting and imaging of tumor cells. *Adv Funct Mater.* 2015;25(34):5472–5478. doi:[10.1002/adfm.201502506](https://doi.org/10.1002/adfm.201502506)
- Zhang J, Ma Y-q, Li N, Zhu J-l, Zhang T, Zhang W, Liu B. Preparation of graphene quantum dots and their application in cell imaging. *J Nanomater.* 2016;2016:9245865. doi:[10.1155/2016/9245865](https://doi.org/10.1155/2016/9245865)
- Wu D, Liu Y, Wang Y, Hu L, Ma H, Wang G, Wei Q. Label-free electrochemiluminescent immunosensor for detection of prostate specific antigen based on aminated graphene quantum dots and carboxyl graphene quantum dots. *Sci Rep.* 2016;6(1):20511. doi:[10.1038/srep20511](https://doi.org/10.1038/srep20511)
- Thakur M, Mewada A, Pandey S, Bhoori M, Singh K, Sharon M, Sharon M. Milk-derived multi-fluorescent graphene quantum dot-based cancer theranostic system. *Mater Sci Eng C.* 2016;67:468–477. doi:[10.1016/j.msec.2016.05.007](https://doi.org/10.1016/j.msec.2016.05.007)
- Yan Y, Chen J, Li N, Tian J, Li K, Jiang J, Liu J, Tian Q, Chen P. Systematic bandgap engineering of graphene quantum dots and applications for photocatalytic water splitting and CO₂ reduction. *ACS Nano.* 2018;12(4):3523–3532. doi:[10.1021/acsnano.8b00498](https://doi.org/10.1021/acsnano.8b00498)
- Yeh T-F, Teng C-Y, Chen S-J, Teng H. Nitrogen-doped graphene oxide quantum dots as photocatalysts for overall water-splitting under visible light illumination. *Adv Mater.* 2014;26(20):3297–3303. doi:[10.1002/adma.201305299](https://doi.org/10.1002/adma.201305299)
- Yeh T-F, Chen S-J, Teng H. Synergistic effect of oxygen and nitrogen functionalities for graphene-based quantum dots

- used in photocatalytic H₂ production from water decomposition. *Nano Energy*. 2015;12:476–485. doi:[10.1016/j.nanoen.2015.01.021](https://doi.org/10.1016/j.nanoen.2015.01.021)
25. Li L, Wu G, Yang G, Peng J, Zhao J, Zhu J-J. Focusing on luminescent graphene quantum dots: current status and future perspectives. *Nanoscale*. 2013;5(10):4015–4039. doi:[10.1039/C3NR33849E](https://doi.org/10.1039/C3NR33849E)
26. Tang L, Ji R, Li X, Teng KS, Lau SP. Size-dependent structural and optical characteristics of glucose-derived graphene quantum dots. *Part Part Syst Charact*. 2013;30(6):523–531. doi:[10.1002/ppsc.201200131](https://doi.org/10.1002/ppsc.201200131)
27. Das SK, Luk CM, Martin WE, Tang L, Kim DY, Lau SP, Richards CI. Size and dopant dependent single particle fluorescence properties of graphene quantum dots. *J Phys Chem C*. 2015;119(31):17988–17994. doi:[10.1021/acs.jpcc.5b05969](https://doi.org/10.1021/acs.jpcc.5b05969)
28. Hummers WS, Offeman RE. Preparation of graphitic oxide. *J Am Chem Soc*. 1958;80(6):1339–1339. doi:[10.1021/ja01539a017](https://doi.org/10.1021/ja01539a017)
29. Trinh TTPNX, Giang NTH, Huong LM, Thinh DB, Dat NM, Trinh DN, Hai ND, Oanh DTY, Nam HM, Phong MT, Hieu NH. Hydrothermal synthesis of titanium dioxide/graphene aerogel for photodegradation of methylene blue in aqueous solution. *J Sci Adv Mater Devices*. 2022;7(2):100433. doi:[10.1016/j.jsamd.2022.100433](https://doi.org/10.1016/j.jsamd.2022.100433)
30. Tian R, Zhong S, Wu J, Jiang W, Wang T. Facile hydrothermal method to prepare graphene quantum dots from graphene oxide with different photoluminescences. *RSC Adv*. 2016;6(46):40422–40426. doi:[10.1039/C6RA00780E](https://doi.org/10.1039/C6RA00780E)
31. Halder A, Godoy-Gallardo M, Ashley J, Feng X, Zhou T, Hosta-Rigau L, Sun Y. One-pot green synthesis of biocompatible graphene quantum dots and their cell uptake studies. *ACS Appl Bio Mater*. 2018;1(2):452–461. doi:[10.1021/acsabm.8b00170](https://doi.org/10.1021/acsabm.8b00170)
32. Amir Faiz MS, Che Azurahaman CA, Raba'ah SA, Ruzniza MZ. Low cost and green approach in the reduction of graphene oxide (GO) using palm oil leaves extract for potential in industrial applications. *Results Phys*. 2020;16:102954. doi:[10.1016/j.rinp.2020.102954](https://doi.org/10.1016/j.rinp.2020.102954)
33. Thi PT, Thang LV, Khai TV, Diem TX, Nghia CNT, Ngan TTT, Tri LM, Vinh NN, Hien NM. Synthesis of Ag/GO nanocomposite with promising photocatalytic ability for reduction reaction of *p*-nitrophenol. *Mater Res Express*. 2021;8:105009. doi:[10.1088/2053-1591/ac2ead](https://doi.org/10.1088/2053-1591/ac2ead)
34. Kumar S, Ojha A K, Ahmed B, Kumar A, Das J, Materny A. Tunable (violet to green) emission by high-yield graphene quantum dots and exploiting its unique properties towards sun-light-driven photocatalysis and supercapacitor electrode materials. *Mater Today Commun*. 2017;11:76–86. doi:[10.1016/j.mtcomm.2017.02.009](https://doi.org/10.1016/j.mtcomm.2017.02.009)
35. Khai TV, Lam DT, Thu VL, Kim WH. A two-step method for the preparation of highly conductive graphene film and its gas-sensing property. *Mater Sci Appl*. 2015;6(11):963–977. doi:[10.4236/msa.2015.611097](https://doi.org/10.4236/msa.2015.611097)
36. Chhabra VA, Kaur R, Kumar N, Deep A, Rajesh C, Kim K-H. Synthesis and spectroscopic studies of functionalized graphene quantum dots with diverse fluorescence characteristics. *RSC Adv*. 2018;8(21):11446–11454. doi:[10.1039/C8RA01148F](https://doi.org/10.1039/C8RA01148F)
37. Dong Y, Shao J, Chen C, Li H, Wang R, Chi Y, Lin X, Chen G. Blue luminescent graphene quantum dots and graphene oxide prepared by tuning the carbonization degree of citric acid. *Carbon*. 2012;50(12):4738–4743. doi:[10.1016/j.carbon.2012.06.002](https://doi.org/10.1016/j.carbon.2012.06.002)
38. Țucureanu V, Matei A, Avram A M. FTIR spectroscopy for carbon family study. *Crit Rev Anal Chem*. 2016;46(6):502–520. doi:[10.1080/10408347.2016.1157013](https://doi.org/10.1080/10408347.2016.1157013)
39. Muzart J. N,N-Dimethylformamide: much more than a solvent. *Tetrahedron*. 2009;65(40):8313–8323. doi:[10.1016/j.tet.2009.06.091](https://doi.org/10.1016/j.tet.2009.06.091)
40. Mandal B, Saha S, Das D, Panda J, Das S, Sarkar R, Tudu B. Supercapacitor performance of nitrogen doped graphene synthesized via DMF assisted single-step solvothermal method. *FlatChem*. 2022;34:100400. doi:[10.1016/j.flatc.2022.100400](https://doi.org/10.1016/j.flatc.2022.100400)
41. Lapekin NI, Anufrieva TV, Ukhina AV, Shestakov AA, Bannov AG. Solvent effect on the NO₂ sensing properties of multi-walled carbon nanotubes. *Chim Techno Acta*. 2022;9(3):20229311. doi:[10.15826/chimtech.2022.9.3.11](https://doi.org/10.15826/chimtech.2022.9.3.11)
42. Gupta V, Chaudhary N, Srivastava R, Sharma G D, Bhardwaj R, Chand S. Luminescent graphene quantum dots for organic photovoltaic devices. *J Am Chem Soc*. 2011;133(26):9960–9963. doi:[10.1021/ja2036749](https://doi.org/10.1021/ja2036749)
43. Kudin K N, Ozbas B, Schniepp H C, Prud'homme R K, Aksay I A, Car R. Raman spectra of graphite oxide and functionalized graphene sheets. *Nano Lett*. 2008;8(1):36–41. doi:[10.1021/nl071822y](https://doi.org/10.1021/nl071822y)
44. Zhu S, Song Y, Zhao X, Shao J, Zhang J, Yang B. The photoluminescence mechanism in carbon dots (graphene quantum dots, carbon nanodots, and polymer dots): current state and future perspective. *Nano Res*. 2015;8(2):355–381. doi:[10.1007/s12274-014-0644-3](https://doi.org/10.1007/s12274-014-0644-3)
45. Yeh T-F, Huang W-L, Chung C-J, Chiang I T, Chen L-C, Chang H-Y, Su W-C, Cheng C, Chen S-J, Teng H. Elucidating quantum confinement in graphene oxide dots based on excitation-wavelength-independent photoluminescence. *J Phys Chem Lett*. 2016;7(11):2087–2092. doi:[10.1021/acs.jpcclett.6b00752](https://doi.org/10.1021/acs.jpcclett.6b00752)
46. Lingam K, Podila R, Qian H, Serkiz S, Rao A M. Evidence for edge-state photoluminescence in graphene quantum dots. *Adv Funct Mater*. 2013;23(40):5062–5065. doi:[10.1002/adfm.201203441](https://doi.org/10.1002/adfm.201203441)
47. Wang L, Zhu S-J, Wang H-Y, Qu S-N, Zhang Y-L, Zhang J-H, Chen Q-D, Xu H-L, Han W, Yang B, Sun H-B. Common origin of green luminescence in carbon nanodots and graphene quantum dots. *ACS Nano*. 2014;8(3):2541–2547. doi:[10.1021/nn500368m](https://doi.org/10.1021/nn500368m)
48. Fang B-Y, Li C, Song Y-Y, Tan F, Cao Y-C, Zhao Y-D. Nitrogen-doped graphene quantum dot for direct fluorescence detection of Al³⁺ in aqueous media and living cells. *Biosens Bioelectron*. 2018;100:41–48. doi:[10.1016/j.bios.2017.08.057](https://doi.org/10.1016/j.bios.2017.08.057)